Materials Research Proceedings **27** (2023) 95-102 https://doi.org/10.21741/9781644902455-12

# Aeroacoustic energy harvesting using relaxor ferroelectric single crystals

Matthew J. Schipper[1,a], David J. Munk[1,b], Jaslyn Gray[1,c], Scott D. Moss[1,d*], Nik Rajic[1,e], Caroline Hamilton-Smith[2,3,f], James Kirkness-Duncombe[2,g], Gareth A. Vio[2,h], Crispin Szydzik[4,i] and Arnan Mitchell[4,j]

[1]Defence Science and Technology Group, Platforms Division, Victoria, Australia

[2]University of Sydney, School of Aerospace Engineering, New South Wales, Australia

[3]DMTC Pty. Ltd., Victoria, Australia

[4]R.M.I.T University, Micro Nano Research Facility, Victoria, Australia

[a]matthew.schipper@defence.gov.au, [b]david.munk@defence.gov.au, [c]jaslyn.gray@defence.gov.au, [d]scott.moss@defence.gov.au, [e]nikolas.rajic@defence.gov.au, [f]caroline.hamiltonsmith@sydney.edu.au, [g]james.kirkness@sydney.edu.au, [h]gareth.vio@uni.sydney.edu.au, [i]crispin.szydzik@rmit.edu.au, [j]arnan.mitchell@rmit.edu.au

* Corresponding author. Tel.: +61-3-9344-2449; fax: +61-3-9626-7089.



**Keywords:** Aeroacoustic, Structural Cavity, Energy Harvesting, Relaxor Ferroelectric Single Crystal, Structural Health Monitoring

**Abstract.** This paper reports on the use of relaxor ferroelectric single crystal for harvesting aeroacoustic energy from the floor of a structural cavity. In particular, this work examines the optimisation of the single crystal transducer geometry to maximise the energy harvested. The transducers used are 0.175 mm thick [011] poled Mn-Pb($Mg_{1/3}Nb_{2/3}$)$O_3$-Pb(Zr,Ti)$O_3$ (or Mn-PMN-PZT) single crystal fibre composite (or SFC). In this study, the SFCs are bonded to the floor of an experimental cavity within a low-speed wind-tunnel with an airspeed of ~ 60 m/s. Air flowing over the cavity creates an oscillatory pressure cycle that is used as a source of harvestable energy. Detailed multiphysics modelling and parametric optimisation were performed, with model predictions well matched to wind-tunnel experimental results. In particular it is shown that, due to the cavity geometry, an SFC mounted on the cavity floor perpendicular to the wind-tunnel flow produces ~4 times more power than an SFC mounted parallel.

## Introduction

Structural health monitoring (SHM) technologies for aerospace are maturing rapidly, and now have the ability to generate the variety, volume, and velocity of data to support digital twins [1-7]. The SHM sensors must withstand environmental instability (e.g. fluctuations in temperature and operational loads etc.), while adding as little mass as possible to maintain aircraft performance [8]. Furthermore, SHM sensors are typically positioned in less accessible locations on an aircraft [9]. Due to these reasons, powering SHM sensors for autonomous operation remains an issue [10]. One proposed solution has been to generate power through harvesting waste energy from the host structure [11], with earlier work exploring the use of relaxor ferroelectric single crystal (RFSC) transduction for harvesting energy from kilo-hertz frequency aircraft structural vibration [10, 12]. In one example involving energy harvesting from the mechanical vibration present on a helicopter transmission, the predicted electrical power available was greater than 11 mW [10]. This amount of harvested vibration energy is viable for powering SHM sensors due to the decreasing power requirements of modern microelectronics [13].

Materials Research Proceedings **27** (2023) 95-102
https://doi.org/10.21741/9781644902455-12

In this paper, an alternative fluid-flow based harvesting approach is examined, in particular the vibration produced by airflow across a structural cavity [14, 15]. In principle, as shown in Fig. 1a, air flowing over a cavity typically creates vortices at the cavity's leading edge. The vortices travel downstream producing a transient high-pressure zone in front of the cavity aft wall, generating an acoustic pressure wave that propagates upstream. This pressure wave acts as feedback creating further vortices at the leading edge, which travel downstream to continue the cycle. This oscillatory pressure-cycle is a source of aeroacoustic energy which produces local structural deflections from which energy can be harvested [16]. In practice, the energy harvested could then be used to power local SHM sensors, for example within the wheel-well or payload-bay of an aircraft.

**Principles of operation**

The primary goal of this work was to use single crystal fibre composite (or SFC) transducers to harvest airflow-induced strain energy from the floor of a structural cavity. Figs. 1b and 1c are photographs of two spring-steel plate arrangements that were employed as the floor of a structural cavity. Bonded at the middle of the plate was an SFC transducer with a Mn-Pb($Mg_{1/3}Nb_{2/3}$)$O_3$-Pb(Zr,Ti)$O_3$ (or Mn-PMN-PZT) piezoelectric element 50 mm long, 25 mm wide, and 0.175 mm thick. The piezoelectric 2-direction of the crystal, which has a large piezoelectric coefficient $d_{32}$ = -1100 pC/N, is parallel to the 50 mm edge of the SFC transducer.

(a)

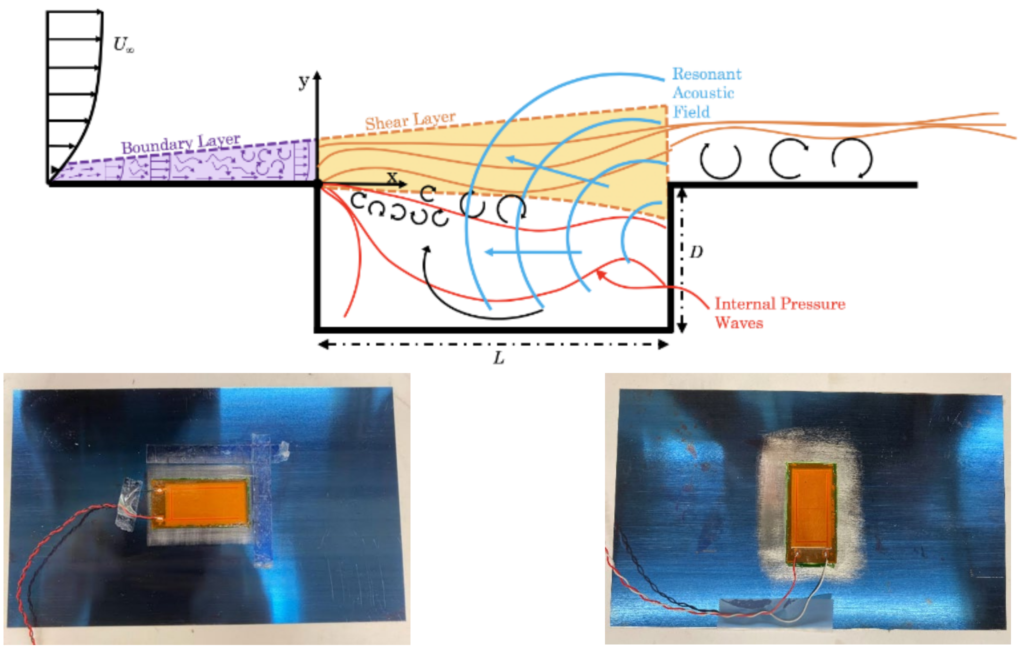


(b) (c)

*Figure 1. (a) Schematic of the wind-tunnel experiment with airflow left-to-right over a cavity, and with the floor of the cavity having length 'L'. Photographs of the SFC transducer (orange) and the spring-steel plate arrangement (blue), which forms the floor of the structural cavity: (b) 'SFC-parallel' with the SFC bonded parallel to the long direction of the plate, and (c) 'SFC-perpendicular' with the SFC bonded perpendicular to the long direction.*

As will be detailed later, a SFC/spring-steel plate arrangement was mounted at the bottom of a structural cavity using 25 mm wide double-sided foam tape. Aeroacoustic pressure variations within the cavity produced periodic deflections of the spring steel plate, producing strain in the SFC transducer from which energy could then be harvested. Multiphysics modelling of the SFC/plate arrangement was performed to guide design optimisation of the energy harvester.

Materials Research Proceedings **27** (2023) 95-102 https://doi.org/10.21741/9781644902455-12

## Modelling

This section will discuss the multiphysics model that was developed to understand the behaviour of the SFC transducer and spring-steel plate arrangement that was employed as the floor of the structural cavity examined in this paper. This model was used to determine the optimal geometry for maximising the energy harvested from the floor of the structural cavity.

The model was produced using commercial software (COMSOL Multiphysics version 5.6), with the main elements being a SFC transducer adhesively bonded at the centre of a 0.381 mm thick, 250 mm long x 132 mm wide spring-steel plate. The adhesive bondline between the SFC and the spring-steel plate was modelled as a 0.3 mm thick layer. Double-side foam tape 1.2 mm thick and 25 mm wide, used to attach the spring-steel plate to the floor of the cavity, was included in the model and located along the edges of the plate. Fig. 2 is a schematic of the modelled geometry and mesh. A fixed constraint was applied along the top face of the tape, and an electrical ground was located at the interface between the adhesive and the SFC transducer. Table 1 summarises the material parameters for the modelled spring-steel plate, bondline adhesive, and double-sided tape. The electromechanical parameters for the SFC transducer material are given in Table 2.

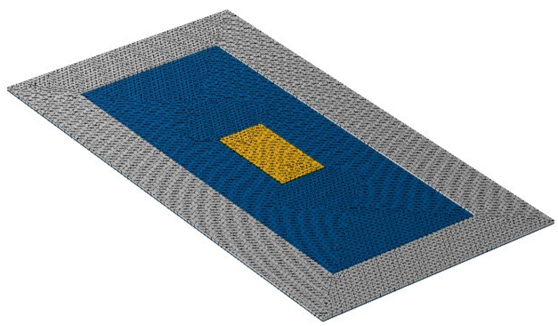

*Figure 2. Example geometry and mesh for a multiphysics model corresponding to Fig. 1b. The orange domain is the modelled SFC transducer, the blue domain is the visible spring-steel plate, and the double-sided foam tape is the light grey domain.*

The model was configured such that the adhesive bondline, the SFC transducer, and modelled piezoelectric-material axes were all capable of being rotated by a specified angle θ shown in Fig. 3. The model was run through a sweep of various angles θ to determine which SFC orientation produced the largest output voltage. For modelling purposes a 1 N point force was applied at the centre of the bottom face of the steel plate and in the direction of the positive z-axis indicated in Fig. 3 (i.e. normal to the page). It is noted that the 1 N point force was roughly equivalent to the peak pressure expected on the spring-steel plate in the wind-tunnel, however since the modelled voltages are relative with respect to θ the exact magnitude of the modelled point force is of no consequence. The model-predicted average surface voltage across the top face of the SFC transducer was recorded as a function of θ, and will be discussed later. It is worth noting that the model was stationary and had ~210k degrees of freedom, and the typical run-time for one instance was 30 seconds on a modern laptop.

*Table 1. Model parameters assumed for spring-steel, bondline adhesive, and double-sided tape.*

| | Density (kg/m$^3$) | Young's Modulus (Pa) | Poisson's ratio |
|---|---|---|---|
| Spring-steel | 7850 | 205 x $10^9$ | 0.28 |
| Bondline adhesive | 1420 | 2.5 x $10^9$ | 0.34 |
| Double-sided tape | 175 | 3.54 x $10^5$ | 0.3 |

Materials Research Proceedings **27** (2023) 95-102
https://doi.org/10.21741/9781644902455-12

*Table 2. Electromechanical parameters assumed for the modelled SFC transducer, with piezoelectric coupling d, relative permittivity $\mathcal{E}$, and compliance s.*

| **Electrical** | | **Mechanical** | |
|---|---|---|---|
| $d_{31}$ (pC/N) | 405 | $s_{11}$ ($10^{-12}$ 1/Pa) | 16.2 |
| $d_{32}$ (pC/N) | -1100 | $s_{12}$ ($10^{-12}$ 1/Pa) | -25.4 |
| $d_{33}$ (pC/N) | 820 | $s_{13}$ ($10^{-12}$ 1/Pa) | 14.9 |
| $d_{24}$ (pC/N) | 145 | $s_{22}$ ($10^{-12}$ 1/Pa) | 69.3 |
| $d_{15}$ (pC/N) | 1997 | $s_{23}$ ($10^{-12}$ 1/Pa) | -43.6 |
| $\varepsilon_{11}$ | 2891 | $s_{33}$ ($10^{-12}$ 1/Pa) | 37 |
| $\varepsilon_{22}$ | 861 | $s_{44}$ ($10^{-12}$ 1/Pa) | 19.5 |
| $\varepsilon_{33}$ | 2570 | $s_{55}$ ($10^{-12}$ 1/Pa) | 179 |
| | | $s_{66}$ ($10^{-12}$ 1/Pa) | 26.8 |
| | | Density (kg/m$^3$) | 7900 |

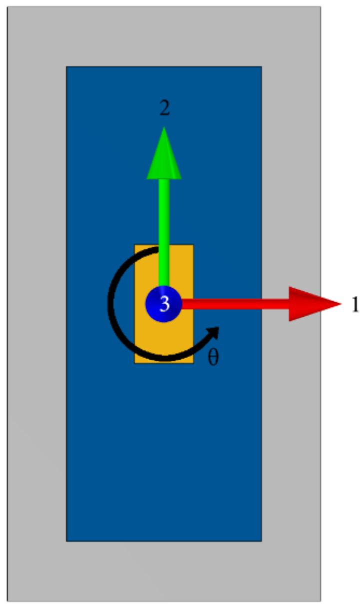


*Figure 3. Orientation of the SFC transducer and the piezoelectric material axes, showing the in-plane rotation θ.*

## Experimental

This section will present a brief overview of the wind-tunnel structural cavity and energy harvesting arrangements used to validate predictions from the multiphysics model detailed earlier.

SFCs were bonded to the centre of the spring-steel plates using a structural adhesive (Clickbond CB359). An SFC/spring-steel plate arrangement was mounted at the bottom of a structural cavity, with the long direction of the plate parallel with the wind-tunnel airflow. In Fig. 1b, designated as 'SFC-parallel', the SFC is oriented parallel to the long direction of the plate, corresponding to $\theta = 0^{\circ}$. In Fig. 1c, 'SFC-perpendicular' has the SFC oriented perpendicular to the long direction of the plate, i.e. rotated through $\theta = 90^{\circ}$. The SFC and spring-steel plate arrangements were experimentally tested by mounting them on the floor of the structural cavity shown in Figs. 4a and 4b. The cavity itself was located at the bottom of the wind-tunnel testing section, which was 4 ft wide by 3 ft high (Fig. 4a).

The cavity was geometrically variable (Fig. 4c), however for the purposes of comparing the experimental results with the model predictions a single cavity length-to-depth ratio (L/D) was chosen. Specifically, an L/D = 1.75 was used, with L = 266 mm and D = 151.6 mm. The cavity width was fixed at 210 mm. The wind-tunnel has a maximum airspeed of 70 m/s (Mach 0.2), with

Materials Research Proceedings **27** (2023) 95-102 https://doi.org/10.21741/9781644902455-12

an airspeed of 60 m/s chosen for experimentation. Air temperature within the wind-tunnel did not exceed 40°C during testing.

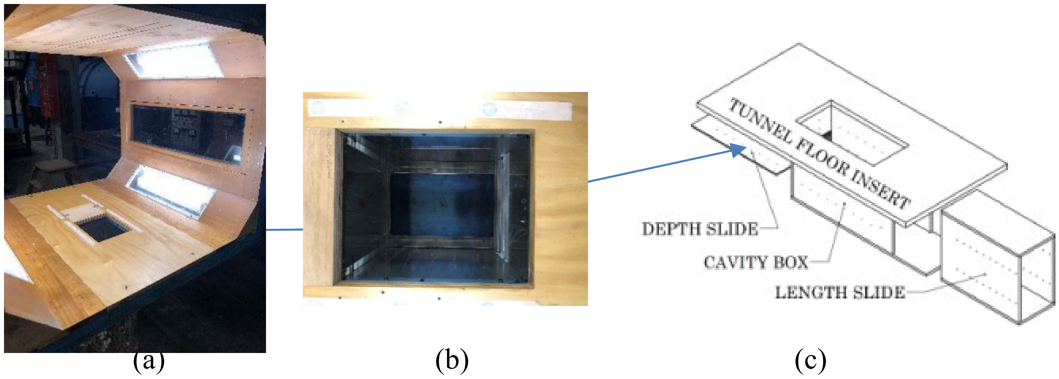


*Figure 4. Photographs of (a) the cavity location within the wind-tunnel, (b) the cavity with spring-steel plate floor with SFC bonded underneath, and (c) schematic of wind-tunnel cavity with variable geometry.*

**Results and discussion**

In this section, the model predictions and the experimental characterisation of the SFC/spring-steel plate arrangements are reported and compared. In particular, the discussion will focus on the SFC-parallel (θ = 0°) versus the SFC-perpendicular oriented (θ = 90°) arrangements.

Fig. 5 plots the modelled open circuit voltage for a SFC/spring-steel plate arrangement, for a range of SFC orientations 0° < θ < 90°. For an SFC orientation of θ = 0° (i.e. SFC-parallel) the open circuit voltage produced is smallest. The voltage increases as θ increases towards 90° (i.e. SFC-perpendicular), where it reaches a maximum value. The modelled voltage extrema are listed in Table 3, with the maximum voltage for the SFC-perpendicular arrangement with θ = 90° being ~2.1 times greater than the minimum for the SFC-parallel arrangement θ = 0°. Since electrical power is proportional to voltage squared, if all else is equal, then the SFC-perpendicular arrangement should generate ~4.4 times the energy compared to that generated by the SFC-parallel arrangement.

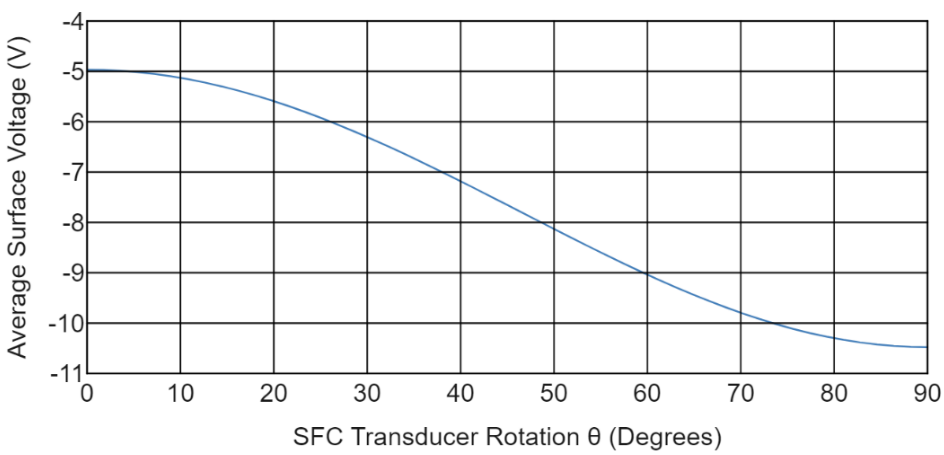


*Figure 5. Model predictions of average open circuit voltage for SFC transducer rotation θ (Fig. 3).*

*Table 3. Extrema for the modelled open circuit voltages produced by an SFC transducer for the SFC-parallel and SFC-perpendicular arrangements (based on Fig. 5).*

| | SFC-parallel | SFC -perpendicular |
|---|---|---|
| Average surface voltage (V) | -4.99 | -10.47 |

The results of the experimental characterisation of the L/D = 1.75 cavity geometry described in the previous section are given in Fig. 6 for both the SFC-parallel and SFC-perpendicular cavity floor arrangements. Fig. 6 plots a sweep of the applied resistive load versus the average electrical power generated, with the maximum power generation occurring when the resistive load matches the electromechanical impedance of the SFC/plate harvesting arrangement. The SFC-perpendicular arrangement generates a maximum power of 19.6 μW with an optimum resistive load of 19.3 kΩ, which is ~3.3 times greater than the 6.0 μW produced by the SFC-parallel arrangement with a 9.6 kΩ load. The measured increase in harvested power of 3.3X (between the perpendicular and parallel arrangements) correlates reasonably well with the 4.4X predicted by the model.

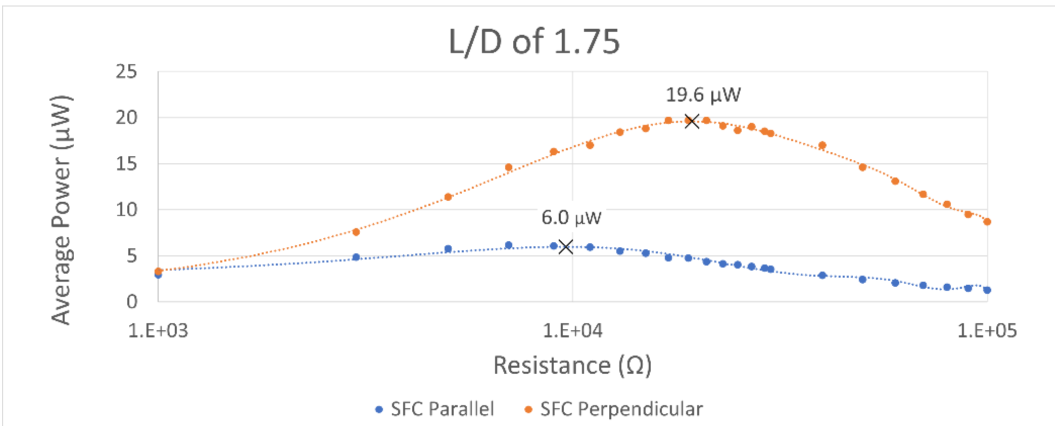


*Figure 6. Measured average-power generated by a SFC transducer as a function of resistive load and for a wind-tunnel cavity with L/D = 1.75. For both arrangements, the interpolated maximum average power is indicated by a black cross (i.e. 'SFC-parallel' arrangement shown in Fig. 1b, and 'SFC-perpendicular' shown in Fig. 1c).*

The increase in energy harvested by the SFC-perpendicular arrangement, compared with the SFC-parallel, can be understood by examining the modelled in-plane strain distributions for the SFC transducer. The strain distribution within an SFC directly correlates with the piezoelectric charge generated, thus determining the amount of mechanical-to-electrical energy transduction. Fig. 7 details the modelled principal strain distribution within the SFC for both the SFC-perpendicular and SFC-parallel arrangements. Note that for clarity the underlying spring-steel plate and adhesive bondline are not shown.

*figure).*

The modelling reveals three important details in the SFC strain distribution:

(i) As indicated by the longer arrows, the SFC-perpendicular arrangement exhibits a larger and more uniform strain distribution in the piezoelectric 2-direction of the SFC. As mentioned previously, the 2-direction is parallel to the long direction of the SFC transducer and possesses a large $d_{32}$ (Table 2), so the SFC-perpendicular arrangement with a larger and more uniform strain distribution should generate a greater amount of piezoelectric charge.

(ii) The SFC-parallel arrangement has a less uniform strain distribution, meaning that more of the SFC electrode area is behaving like a parasitic parallel capacitor soaking up charge from the strained region and thus lowering the effective voltage on the SFC electrode (i.e. $V_{SFC} = Q_{SFC}/C_{SFC}$ reduces as $C_{SFC}$ increases).

Materials Research Proceedings **27** (2023) 95-102
https://doi.org/10.21741/9781644902455-12

(iii) For the SFC-parallel arrangement, the direction of the principal strains in the lower-strained SFC regions are rotated 90° with respect to the principal strains in the higher-strained region. This means that the higher-strained regions are in tension in the 2-direction with $d_{32}$ = -1100 pC/N, whereas the lower-strained regions are in tension in the 1-direction with $d_{31}$ = +480 pC/N; this will result in charge cancellation due to the differing signs of $d_{32}$ and $d_{31}$. For these three reasons, the aggregate charge generated by the SFC-perpendicular arrangement is expected to be significantly greater than that for the SFC-parallel arrangement. Future work will examine the optimisation of the SFC geometry to maximise the in-plane strain and its uniformity.

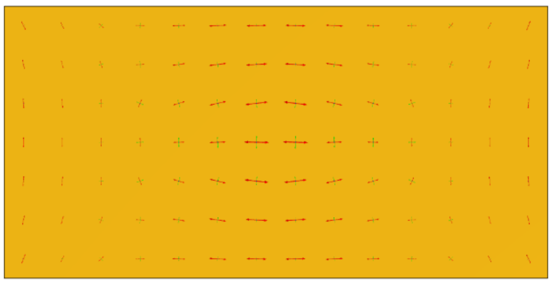

(a)

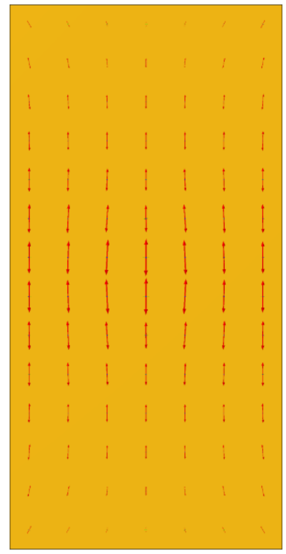

(b)

*Figure 7. Plot of the modelled principal strain distributions for the (a) SFC-parallel, and (b) SFC-perpendicular arrangements. The arrow lengths are proportional to the amplitude of the modelled SFC transducer strain. The model assumes an arbitrary 1 N load normal to centre of the SFC/spring-steel plate arrangements (with the underlying spring-steel plate not shown in this*

## Conclusion

This paper reports on an approach for harvesting energy from the floor of a structural cavity arrangement using relaxor ferroelectric single crystals. Airflow across the cavity generates an aeroacoustic structural response from which energy is harvested using a [011] poled Mn-PMN-PZT single crystal fibre composite (SFC) transducer. The SFC transducer was bonded to a 0.381 mm thick, 250 mm long x 132 mm wide spring-steel plate. The plate was mounted to the floor of a structural cavity with dimensions length L = 266 mm and depth D = 151.6 mm, with L/D = 1.75. The cavity width was fixed at 210 mm. Multiphysics modelling of the orientation of the SFC transducer was performed, indicating that the SFC transducer bonded perpendicular to the long direction of the cavity floor was optimal. Model predictions were validated via low-speed wind-tunnel testing, with the maximum power harvested being 19.6 µW from a 60 m/s airflow over the structural cavity. The modelled in-plane strain distributions within the SFC transducers were examined, with the principal strains found to be larger and more uniform when the SFC was bonded in the perpendicular arrangement.

## Acknowledgements

The authors gratefully acknowledge the assistance of the DSTG Battle Ready Platforms program, the DSTG IEP program, and the Advanced Piezoelectric Materials and Applications Program supported by DMTC Limited (Australia) and funded by DSTG through the Next Generation Technologies Fund. The authors would also like to thank Mr. Daniel Bitton.

Materials Research Proceedings **27** (2023) 95-102 https://doi.org/10.21741/9781644902455-12

**References**

[1] N. Rajic, S. Galea, Thermoelastic stress analysis and structural health monitoring: an emerging nexus, Struct. Health Monitoring. 14 (2015) 57–72. https://doi.org/10.1177/1475921714548936
[2] A. Baker, N. Rajic, C. Davis, Towards a practical structural health monitoring technology for patched cracks in aircraft structure, Composites Part A: Appl. Sci. Manuf. 40 (2009) 1340–1352. https://doi.org/10.1016/j.compositesa.2008.09.015
[3] C. Boller, F.-K. Chang, Y. Fujino, Encyclopedia of Structural Health Monitoring, John Wiley & Sons, New Jersey, 2009. https://doi.org/10.1002/9780470061626
[4] V. Ewald, R. S. Venkat, A. Asokkumar, R. Benedictus, C. Boller, R. M. Groves, Perception modelling by invariant representation of deep learning for automated structural diagnostic in aircraft maintenance: A study case using Deep SHM, Mech. Sys. Signal Proc. 165 (2022) 108153. https://doi.org/10.1016/j.ymssp.2021.108153
[5] N. Rajic, D. Rowlands, Thermoelastic stress analysis with a compact low-cost microbolometer system, Quant. Infra. Thermo. J. 10 (2013) 135-158. https://doi.org/10.1080/17686733.2013.800688
[6] Y.C. Zhu, D. Wagg, E. Cross, R. Barthorpe, Real-Time Digital Twin Updating Strategy Based on Structural Health Monitoring Systems, Model Valid. Uncert. Quant. 3 (2020) 55-64.
[7] C. Cremona, J. Santos, Structural Health Monitoring as a Big-Data Problem, Struct. Eng. Int. 28 (2018) 243-254. https://doi.org/10.1007/978-3-030-47638-0_6. https://doi.org/10.1080/10168664.2018.1461536
[8] S. Moss, A. Barry, I. Powlesland, S. Galea, G.P. Carman, A low profile vibro-impacting energy harvester with symmetrical stops, Appl. Phys. Lett. 97 (2010) 234101. https://doi.org/10.1063/1.3521265
[9] S. Moss, I. Powlesland, S. Galea, G. Carman, Vibro-impacting power harvester, Proc. SPIE 7643 (2010) 76431A. https://doi.org/10.1117/12.848897
[10] D.J. Munk, E.J.G. Ellul, S.D. Moss, An approach for the design and validation of high frequency vibration energy harvesting devices, Smart Mater. Struct. 30 (2021) 065018. https://doi.org/10.1088/1361-665X/abfb41
[11] A. Erturk, D.J. Inman, Piezoelectric Energy Harvesting: Modelling and Application, 1st ed., John Wiley & Sons, New Jersey, 2011. https://doi.org/10.1002/9781119991151
[12] T.F. Doughney, S.D. Moss , D.Blunt, W. Wang, H.J. Kissick, Relaxor ferroelectric transduction for high frequency vibration energy harvesting, Smart Mater. Struct. 28 (2019) 065011. https://doi.org/10.1088/1361-665X/ab15a5
[13] C. Piguet, Low-power processors and systems on chips, CRC Press, Boca Raton, 2018. https://doi.org/10.1201/9781315220581
[14] R. Montheard, M. Baeur, V. Boitier, X. Dollat, N. Nolhier, E. Piot, C. Airiau, J.-M. Dilhac, Coupling supercapacitors and aeroacoustic energy harvesting for autonomous wireless sensing in aeronautics applications, Energy Harvesting and Sys. 3 (2016) 265-276. https://doi.org/10.1515/ehs-2016-0003
[15] M. Hamlehdar, A. Kasaeian, M.R. Safaei, Energy harvesting from fluid flow using piezoelectrics: a critical review, Renewable Energy. 143 (2019) 1826-1838. https://doi.org/10.1016/j.renene.2019.05.078
[16] D.J. Munk, C.O. Hamilton Smith, J.M. Kirkness-Duncombe, J.D. Flicker, S.D. Moss, G. A. Vio, Energy harvesting from flow unsteadiness within a cavity, in preparation.